Monazite analysis; from sample preparation to microprobe age dating and REE quantification

by *N.C. Scherrer, M. Engi, E. Gnos, V. Jakob* and *A. Liechti*

Abstract

Despite the recognized importance of monazite in geochronology and petrology, a range of fundamental analytical and preparational problems remains. For example, chemical Th-U-Pb dating of monazite requires special lead-free sample preparation. This is achieved efficiently and at high quality with specially developed grooved ND-PE polyethylene polishing disks. Techniques useful in locating and characterizing monazite are evaluated. Back scattered electron imaging is an effective way to determine zonation patterns, particularly with respect to thorium. Quantitative analysis of monazite by EMP is delicate and time consuming. A whole series of X-ray peak interferences has been ignored in published work. For example, for monazite containing 12% Th, the commonly disregarded interference of Th Mz on Pb Mα causes an overestimation of 11% (relative) in Pb. This propagates to an age overestimation of ~ 50 Ma for a sample of 400 to 500 Ma in age. A judicious choice of X-ray peaks used in quantitative EMP analysis avoids or minimises peak overlap for all elements, including REE. Only for U a correction factor is required: U wt%$_{corrected}$ = U wt%$_{measured}$ − (0.0052 * Th wt%$_{measured}$) based on the analytical lines U Mb and Th Ma.

Keywords: EMPA, REE, monazite, polishing, sample preparation, chemical dating, Th-U-Pb dating.

Introduction

Monazite is increasingly recognized as a powerful mineral for age dating in a wide variety of igneous (MOUGEOT et al., 1997), metamorphic (BINGEN and VAN BREEMEN, 1998; BRAUN et al., 1998; KINGSBURY et al., 1993; PAQUETTE et al., 1999; PARRISH, 1990; SUZUKI and ADACHI, 1994) and even diagenetic (EVANS and ZALASIEWICZ, 1996) environments. Monazite does not "incorporate" appreciable common lead during growth and thus all of its lead is radiogenic, from the decay of Th and U. This eliminates the need for an isotopic correction for common lead. The possibility to date monazite older than ~ 200 Ma with the electron microprobe (EMP), a non-destructive, in-situ, high-resolution, and accessible method, has enhanced the mineral's popularity as a chronometer. Various other methods (e.g. ion microprobe, LA-ICP-MS, XRF) allow dating of geologically young monazite, giving this mineral good potential for solving geochronological problems over a wide range of time. Problems identified in monazite geochronology range from sample preparation (contamination with lead) to analytical complications (X-ray line interference) to complex processes during and following the formation of monazite (^{230}Th disequilibrium, Pb loss, U excess, single grain zoning).

Relatively little is known about monazite forming reactions despite its importance for a better interpretation of P-T-t data. To decipher such reactions, quantitative microanalysis of monazite in thin section is indispensible. ANDREHS and HEINRICH (1998) demonstrated the use of monazite in temperature-calibrated geochronology, requiring complete quantitative analysis of coexisting xenotime and monazite. On reviewing published EMP analyses of monazite, considerable differences in the quality of the analyses have become apparent.

The present paper addresses mainly technical aspects of finding, analysing and chemically dating monazite. We report techniques specifically developed for sample preparation, characterization and analysis of monazite. While monazite is a fre-

Mineralogisch-petrographisches Institut, Universität Bern, Baltzerstrasse 1, CH-3012 Bern, Switzerland.
<engi@mpi.unibe.ch>

quent accessory in various rock types, it is by no means easy to find and identify by the untrained eye. We evaluated a range of techniques to locate this mineral in context and present information on their relative merits.

Sample preparation

Th-U-Pb dating by the EMP requires lead-free polishing. While this can be time consuming for large series, a method is presented to achieve excellent polish with an efficiency competitive to conventional polishing techniques.

Conventional lead disks are unsuitable for the production of thin sections for Th-U-Pb analysis on the EMP because they deposit lead at grain boundaries, filling in surface irregularities and thus contaminating the sample. Lead-free polishing disks made of ND-PE Polyethylene have achieved astonishing results, though only after special treatment of the abrasive surface. Using a Schaublin lathe, a spiral groove of 0.1 mm depth was cut at 75 rotations per minute and 150 mm/min radial progression (Fig. 1). This reduced the total polishing time from days to less than 3 hours. It proved necessary to make adjustments to the sequence of abrasives used; the currently most successful procedure is listed in table 1. The quality of surface polish achieved by this method is equivalent to conventional techniques (using a lead disk), with comparable preparation efficiency.

Finding monazite

A range of methods has been tried with variable success. Cathode luminescence and UV luminescence, applicable to zircon, are unsuitable. Monazite does not luminesce with either technique. By far the most efficient and practical method is scanning (lead-free) polished thin sections in BSE-mode, using the EMP. The methods evaluated are outlined and detailed recommendations are given.

OPTICAL MICROSCOPY

Petrographic microscopy of thin sections provides an efficient way to find heavy minerals in their textural context. Detecting monazite with reasonable certainty, however, requires experience, and even with all that, monazite is not always clearly distinguishable from zircon, allanite, xenotime or titanite. Some practical hints are given on distinctive characteristics of the various phases, always in comparison with monazite.

Zircon: in reflected light, zircon is distinctly brighter than monazite; zircon is often euhedral with elongate shapes and occurs mostly as single grains whereas monazite tends to show rounded or irregular shapes and often occurs as clusters or in trails; the low uranium and thorium content in zircon implies that radiation damage to the host minerals becomes visible only if the rocks exceed several hundred million years in age.

Allanite has low interference colors (1st order grey to brown) whereas monazite generally shows
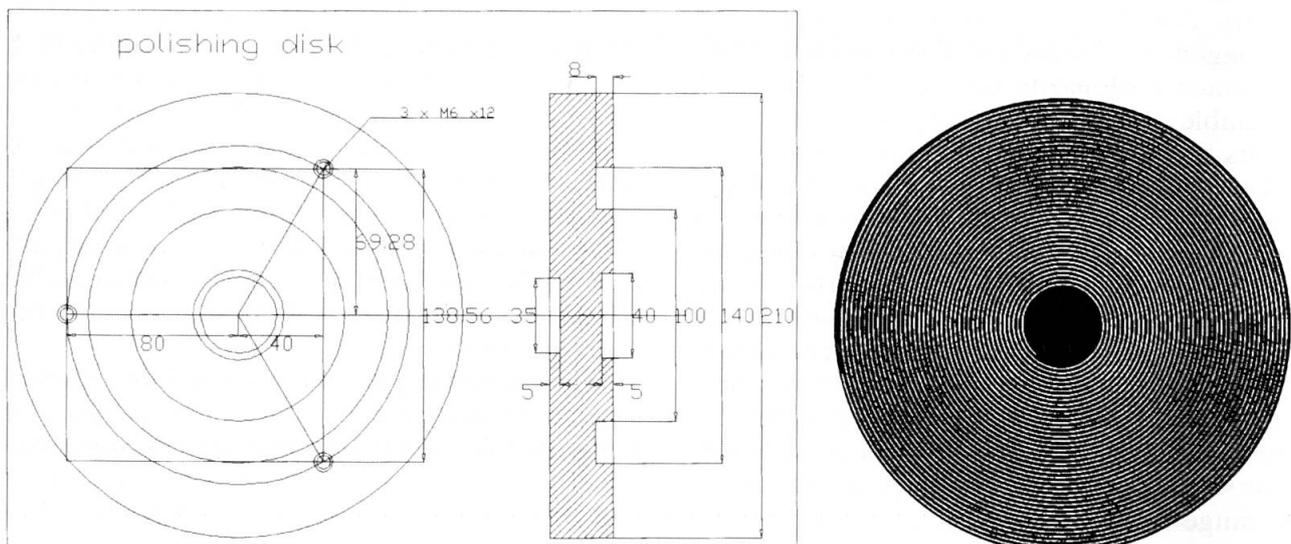

Fig. 1 Plan of the ND-PE Polyethylene disks with spiral groove pattern developed for lead-free thin section preparation at the University of Bern. Measurements are in mm.

Tab. 1 Overview of lapping and polishing procedure.

LAPPING			
Steps	Disk	Abrasive	Time in min
1	Cast iron	SiC 600 plus water	30
2	Glass plate (by hand)	SiC 800 plus water	1 to 2
POLISHING			
Steps	Disk	Abrasive	Time in min
1*	PE disk with spiral grooves	Stähli AWS-WS-4-8/19 plus AWS-DS-5-8 10.0	2 × 30
2*	PE disk with spiral grooves	Stähli AWS-WS-2-3/20 plus AWS-DS-2-4 10.0	2 × 30
3*	PE disk with spiral grooves	Stähli AWS-WS-1/20 plus AWS-DS-0.75-1.5 10.0	1–2 × 30
* after each step, the PE disks are roughened with a diamond ring			

distinctly higher ones (third order blue to fourth order green or yellow); simple twinning is common in allanite, not so in monazite which may exhibit multiple twinning. Euhedral grain shapes and color zoning are typical features of allanite, and grain sizes exceeding 100 μm are common; pleochroic halos around allanite (and monazite!) are common in biotite and chlorite, even in rocks younger than 50 Ma.

Xenotime is virtually indistinguishable from monazite, apart from the lack of halos due to low uranium and low thorium contents.

Titanite similarly occurs as trails; in general, it is easily distinguished in transmitted light showing darker body colors.

Monazite is colorless or faintly colored from yellow to brown, but is clearly distinguishable from rutile. Pleochroic halos in biotite, chlorite and cordierite are a characteristic but non-exclusive feature; interference colors (3rd order) may resemble epidote, zircon or small titanite. Grain shapes and textural relations of monazite vary widely, especially in metamorphic rocks (Fig. 2). Petrographic observation supplemented by electronic imaging (SEM, EMP, see below) provide the best means to identify likely interpretations of geochronologic data. Understanding local phase relations and reaction textures (e.g. BEA and MONTERO, 1999; BINGEN and VAN BREEMEN, 1998; FINGER et al., 1998; SPEAR and PARRISH, 1996) is crucial in linking metamorphic processes to monazite ages.

OPTICAL SPECTROSCOPY

A technique applied to identify gemstones, each having characteristic absorption bands within the visible spectrum. Neodymium, a common constituent in monazite, has absorption lines at 580, 525 and 514 nm (BERNSTEIN, 1982) and these are visible to the trained eye, provided monazite grains have diameters in excess of 60 μm. The method is applicable to grain mounts or thick sections.

ALPHA SPUTTERING

This method relies on the emission of alpha particles from the radioactive decay of uranium and thorium. Since monazite may contain up to 30 wt% thorium, sufficient alpha particles are emitted to produce alpha tracks on an alpha emission sensitive film. This is achieved by exposing lightly polished rock sections to Kodak LR115 type 1 film for two weeks or longer. Development times are up to six hours. Unfortunately, metamorphic monazite commonly has Th contents of around 2 to 15 wt%, which is insufficient to produce visible alpha tracks within a month. The method is better suited for minerals such as uraninite (Fig. 3) or thorianite.

SCANNING ELECTRON MICROSCOPE (SEM)

Prerequisites are lead-free polished thin sections coated with either carbon, aluminum or beryllium. The SEM allows complete thin sections to be scanned quite efficiently (magnification 20 ×) and provides positive identification of monazite by EDS (energy dispersive spectrometry) analysis. By adjusting the brightness and contrast on the screen, zircon and other bright phases such as ilmenite are easily filtered out such that the remaining bright spots can be examined to distinguish monazite from xenotime with a quick EDS analysis. The imaging features can produce quick digital images at various scales for recognition under the optical microscope. A major drawback of the SEM is the missing optical microscope.
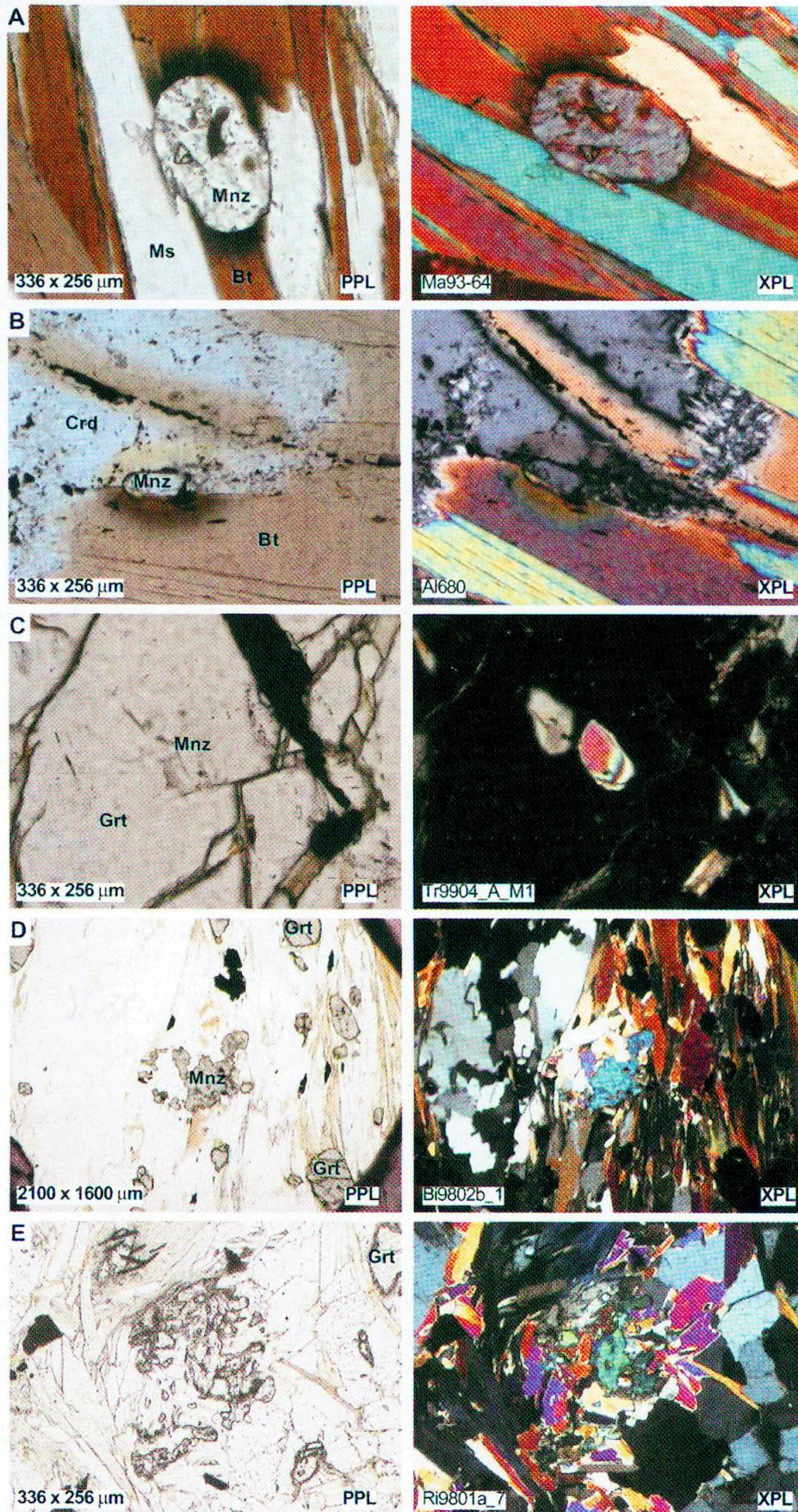
Fig. 2   Monazites in metapelitic rocks under the optical microscope: typical morphologies. Left column: plain polarizers; on right: crossed nicols, same scale.
(A) Single grain monazite with typical rounded shape and pleochroic halo in biotite. (B) Characteristic yellowish pleochroic halo in cordierite and dark halo in biotite. (C) Monazite inclusion in garnet. (D) Pre-kinematic monazite
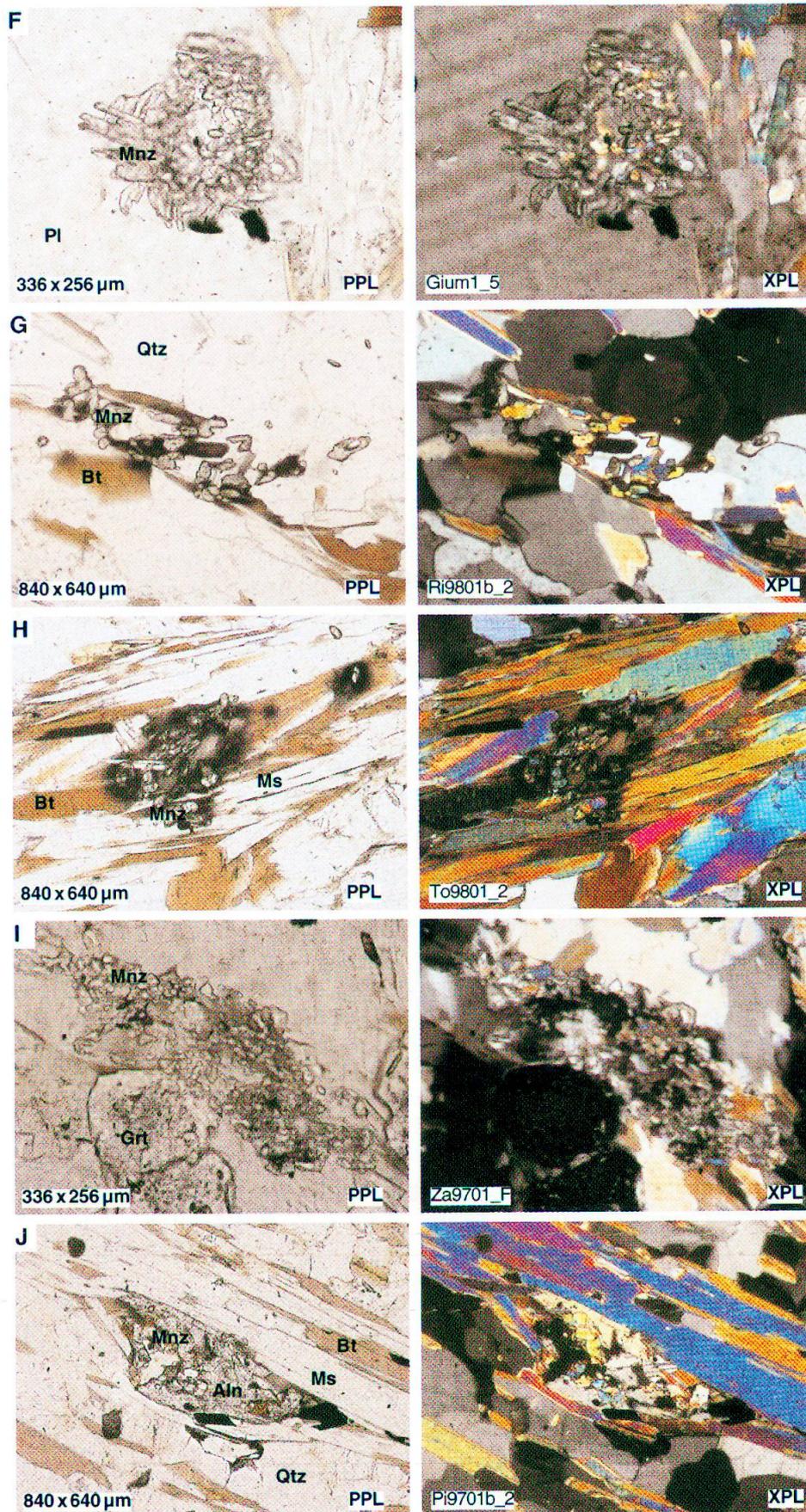
blast in garnet-bearing mica schist. (E) Monazite relic. (F) Vermicular monazite: close arrangement of round or elon-gated fine-grained monazite. (G) Monazite "trail": "stretched" cluster of small rounded monazite grains. (H) Loose cluster of small rounded monazite grains in biotite. (I) Large cluster of monazite with larger fragments. (J) Monazite associated with allanite.

Fig. 3 Alpha tracks emitted from a uraninite bearing sample recorded on Kodak LR115 type 1 film. The tracks can be viewed under a normal petrographic microscope (A1, B1). A2 and B2 are contrast-enhanced images (b&w).

ELECTRON MICROPROBE (EMP)

Again, thin sections must be prepared with lead-free polishing and carbon coated. The EMP combines all of the advantages of finding monazite, imaging zonation patterns, quantification and chemical Th-U-Pb dating of old monazite (> 200 Ma, or younger if thorium contents are exceptionally high). Monazite is easily and efficiently localized and mapped using the BSE feature on an electron microprobe.

Tab. 2 Electron microprobe settings from the literature applied to the quantitative analysis of monazite. Note that the critical ionisation energies of the L-lines of elements La to Lu range from 6 keV to 11 keV. Ideally, the accelerating voltage should be 3 to 5 times the ionisation energy, i.e. at least 20 kV.

kV	nA	Reference
15	10	GRATZ and HEINRICH, 1997; PODOR and CUNEY, 1997
15	20	DELLA VENTURA et al., 1996; DE PARSEVAL et al., 1997
15	40	VAN EMDEN et al., 1997
15	100	BINGEN and VAN BREEMEN, 1998
15	150	SUZUKI and ADACHI, 1994; CROWLEY and GHENT, 1999
15	250	FINGER and HELMY, 1998; FINGER and BROSKA, 1999
15	100	MONTEL et al., 1996
20	10	MANNUCCI et al., 1986; DEMARTIN et al., 1991
20	20	FIALIN et al., 1997
20	40	FRANZ et al., 1996; RHEDE, GFZ Potsdam, 1999
20	50	KINGSBURY et al., 1993; SIMMAT, Uni Bonn, 1999
20	75	RAPP and WATSON, 1986
20	100	COCHERIE et al., 1998
25	130	MONTEL et al., 1994

EMP quantitative analysis of monazite and xenotime

Quantitative analysis of monazite and xenotime is not trivial and should be planned with care. The considerable number of Rare Earth elements occurring in monazite and xenotime requires careful selection of X-ray lines such that interferences can be kept to a minimum. On examining the recent literature to find EMP settings suitable for monazite analysis, one finds a whole range of analytical strategies (Tab. 2). While there exist several methods to correct for peak overlaps (ÅMLI and GRIFFIN, 1975; DONOVAN et al., 1993; FIALIN et al., 1997; ROEDER, 1985), it appears to be more sensible to choose lines with negligible interference (EXLEY, 1980), even at the cost of some extra analysis time. Well characterized standard materials are essential and, ideally, synthesized REE-phosphates should be used (refer to JAROSEWICH and BOATNER, 1991). Synthesized glass standards by DRAKE and WEILL (1972) may be used for minor elements or as secondary standards. With respect to Th-U-Pb dating, ThP_2O_7, a synthesized thorium phosphate, achieved better results than ThO_2, while UO_2 is preferable to elemental U. Concerning the calibration of Pb, either a well

Tab. 3 Absolute background positions recommended by WILLIAMS (1996) for Rare Earth element analysis. Additional positions (this study) are marked with an asterisk*.

LiF	PET
38500	29775
41336*	30735
45400	40970*
51700	45865*
55650	50890*
64750	62510*
67170	

Tab. 4 Critical elements in monazite and xenotime analysis. Data is based on compositions for monazite and xenotime listed in table 5, and on the program VIRTUAL WDS (REED and BUCKLEY, 1996). Problematic X-ray lines are highlighted. Interference ratios have been calculated for the given mineral compositions and will vary with differing monazite or xenotime compositions (more or less significant). Interference can be ignored if none of the overlapping elements are present, but not otherwise. Xenotime has been included to point at potential problems with Gd thermometry after GRATZ and HEINRICH (1997). References: 1) ANDREHS and HEINRICH, 1998; 2) COCHERIE et al., 1998; 3) CROWLEY and GHENT, 1999; 4) DELLA VENTURA et al., 1996; DEMARTIN et al., 1996; 5) DEMARTIN et al., 1991; 6) FIALIN et al., 1997; 7) FINGER and BROSKA, 1999; 8) FINGER and HELMY, 1998; 9) FRANZ et al., 1996; 10) GRATZ and HEINRICH, 1997; 11) MANNUCCI et al., 1986; 12) MONTEL et al., 1994; 13) PODOR and CUNEY, 1997; 14) RAPP and WATSON, 1986; 15) WILLIAMS et al., 1999.

Favored line	X-tal	Wave	I cps	Inferior lines	X-tal	Wave	I cps	Interferences (order)	Wave	I cps	Ratio†	wt% overl.	Elem. wt%	Significance	References (refer to caption)
P Kα1 Mnz	PET	70343	124329					Y Lb1 (1)	71005	36	0.0003	0.004	12.373	–	4); 9); 13); 14)
				P Kα1	TAP	23956	540638	Y Lb1 (1)	24182	2046	0.0038	0.047		–	6)
P Kα1 Xe	PET	70343	158956					Y Lb1 (1)	71005	619	0.0039	0.06	15.521	–	
				P Kα1	TAP	23956	691209	Y Lb1 (1)	24182	35449	0.0513	0.796		**	
La Lα1 Mnz	LiF	66202	10046								0	0	9.757	–	9); 14)
				La Lα1	PET	30468	65962	Nd Ll (1)	30600	839	0.0127	0.124		*	4); 5); 11); 13)
Pr Lb1 Mnz	LiF	56091	2267					La Lb2_15 (1)	57216	16	0.0146	0.031	2.155	*	2); 9)
								Ce Lb6 (1)	56662	17					
				Pr Lb1	PET	25819	8120	La Lb2_15 (1)	26334	74	0.0507	0.109		**	4)
								Ce Lb3 (1)	26407	338					
				Pr Lα1	PET	28152	15214	La Lb1 (1)	28106	25671	1.6873	3.636		***	5); 11)
Nd Lb1 Mnz	LiF	53809	8093					Dy Ll1 (1)	53615	5	0.0101	0.069	6.806	–	2); 9)
								Ce Lb2 (1)	54855	77					
				Nd Lα1	LiF	58863	9956	Ce Lb1 (1)	58515	153	0.0154	0.105		*	4); 6)
								Ce Lb4 (1)	58356	0					
				Nd Lα1	PET	27094	56434	La Lb3 (1)	27571	359	0.0684	0.465		**	5); 11)
								Ce Lb1_4 (1)	26917	3500					
				Nd Lb1	PET	24768	22081	La Lg1 (1)	24505	45	0.0251	0.171		*	
								Ce Lb2_15 (1)	25241	371					
								Sm Lα1 (1)	25140	139					
Sm Lb1 Mnz	LiF	49623	2989					Er Ll1 (1)	50044	0	0.011	0.021	1.927	*	4); 6); 9)
								Ce Lg1 (1)	50881	15					
								Nd Lb2 (1)	50565	15					
								Tb Lα1 (1)	49088	3					
				Sm Lα1	LiF	54624	3702	Ce Lb2 (1)	54855	312	0.0867	0.167		**	2); 14)
								Pr Lb3 (1)	55066	9					
Gd Lb1 Mnz	LiF	45864	2415					Ho Lα1 (1)	45822	75	0.0311	0.042	1.351	Ho dependent	1); 9); 10)
				Gd Lα1	LiF	50831	3289	Ce Lg1 (1)	50881	1926	0.6564	0.887		***	4)
								La Lg3 (1)	50709	135					
								Nd Lb2 (1)	50565	98					
Gd Lα1 Xe	LiF	50831	3655					Ce Lg1 (1)	50881	3	0.0011	0.002	1.471	–	
								La Lg3 (1)	50709	0					
								Nd Lb2 (1)	50565	1					
				Gd Lb1	LiF	45864	2683	Ho Lα1 (1)	45822	2860	1.066	1.568		***	1); 9); 10)
Tb Lb1 Mnz	LiF	44128	351					Er Lα1 (1)	44313	19	0.0769	0.014	0.178	Er dependent **	1); 9); 10)
								Sm Lg5 (1)	44202	8					
				Tb Lα1	LiF	49085	490	Sm Lb1 (1)	49623	18	0.1469	0.026		**	
								La Lg4 (1)	49277	16					
								Ce Lg10 (1)	48796	30					
								Pr Lg1 (1)	48700	8					
Tb Lα1 Xe	LiF	49085	2137					Sm Lb1 (1)	49623	1	0.0005	0	0.79	–	
								La Lg4 (1)	49277	0					
								Ce Lg10 (1)	48796	0					
								Pr Lg1 (1)	48700	0					
				Tb Lb1	LiF	44128	1530	Er Lα1 (1)	44313	493	0.3222	0.255		***	1); 9); 10)
								Sm Lg5 (1)	44202	0					
Er Lα1 Mnz	LiF	44314	378					Tb Lb1 (1)	44128	51	0.1561	0.021	0.132	Tb dependent **	
								Sm Lg5 (1)	44202	6					
								Nd Lg3 (1)	44613	2					
				Er Lb1	LiF	39426	243	Gd Lg1 (1)	39548	99	0.4239	0.056		***	9)
								Dy Lb5 (1)	39468	4					
Lu unresolved!				Lu Lα1	LiF	40222	60	Sm Lg4 (1)	39907	2	3.4667	0.055	0.016	***	1); 9)
								Gd Lg1 (1)	39548	1					
								Ho Lb3 (1)	40241	12					
								Dy Lb2 (1)	40325	193					
				Lu Lb1	LiF	35356	31	Yb Lb2 (1)	35155	2	1.6774	0.027		***	
								Ho Lb1 (1)	35202	2					
								Dy Lg3 (1)	35187	45					
								Tb Lg4 (1)	35427	3					
Pb Mb1 Mnz	PET	58020	561					U Mz2	57707	2	0.0036	0.001	0.269	–	
				Pb Mα1	PET	60393	805	Y Lg2_3	60367	22	0.1106	0.03		**	2); 3); 7); 8); 12); 14); 15)
								Th Mz1,2	59968	67					
U Mb1 Mnz	PET	42475	3795					Th Mg1 (1)	42052	286	0.0754	0.042	0.555	**	9); 12)
				U Mα1	PET	44692	2656	Th Mb1 (1)	45046	791	0.2997	0.166		***	2); 7); 8)
								Ce Lg2-3 (2)	44695	5					

† ratio derived from (sum of interfering counts)/(peak counts of line of interest)*100 = overlap in percent

= overestimation of element in wt% for the composition given

from mineral composition table

– no overlap; - overlap ≤ 1%; * overlap 1 to 4%; ** overlap 4 to 29%; *** overlap ≥ 30%

characterized crocoite or vanadinite should be given preference over galena, avoiding interference of S on Pb.

Though rarely published, background positions are critical. Because of the very closely spaced X-ray lines of the REE, it is preferable to use global rather than local background positions free of interferences, as suggested by WILLIAMS (1996). Experimentation has shown that for elements from Pr to U it is best to measure upper and lower background on the two closest overlap-free positions (according to Tab. 3) surrounding the peak of interest.

Table 4 summarizes the most relevant overlaps, pointing at the relative overestimation induced by analysis of the inferior line(s). With respect to Th-U-Pb dating of monazite by means of the EMP, it should be interesting to know that neither U Ma nor U Mb are free of significant peak interference related to the Th content. None of the referenced papers indicate correction proce-

dures. To derive a simple correction procedure based on the analytical lines Th Ma and U Mb, theoretical counts were simulated on VIRTUAL WDS (REED and BUCKLEY, 1996), using monazite compositions with varying amounts of Th. The ratio of interest, determined to be 0.0052 (Tab. 7), is the intensity of Th Mg at the peak position of U Mb over the intensity of the analyzed line Th Ma. Even more relevant with respect to Th-U-Pb dating is the choice between Pb Ma and Pb Mb. While no correction is required to Pb Mb, Pb Ma should be corrected for interfering Th Mz and Y Lg, the former being the more relevant to monazite, commonly being high in Th and low in Y (Fig. 4, Tab. 4). This tends to be neglected (i.e. COCHERIE et al., 1998; CROWLEY and GHENT, 1999; FINGER and BROSKA, 1999; FINGER and HELMY, 1998; MONTEL et al., 1994; SUZUKI and ADACHI, 1994; WILLIAMS et al., 1999). Uncertainties are relatively high in Th-U-Pb age determinations by EMP, being quite sensitive to variations in Pb. It is thus essential to
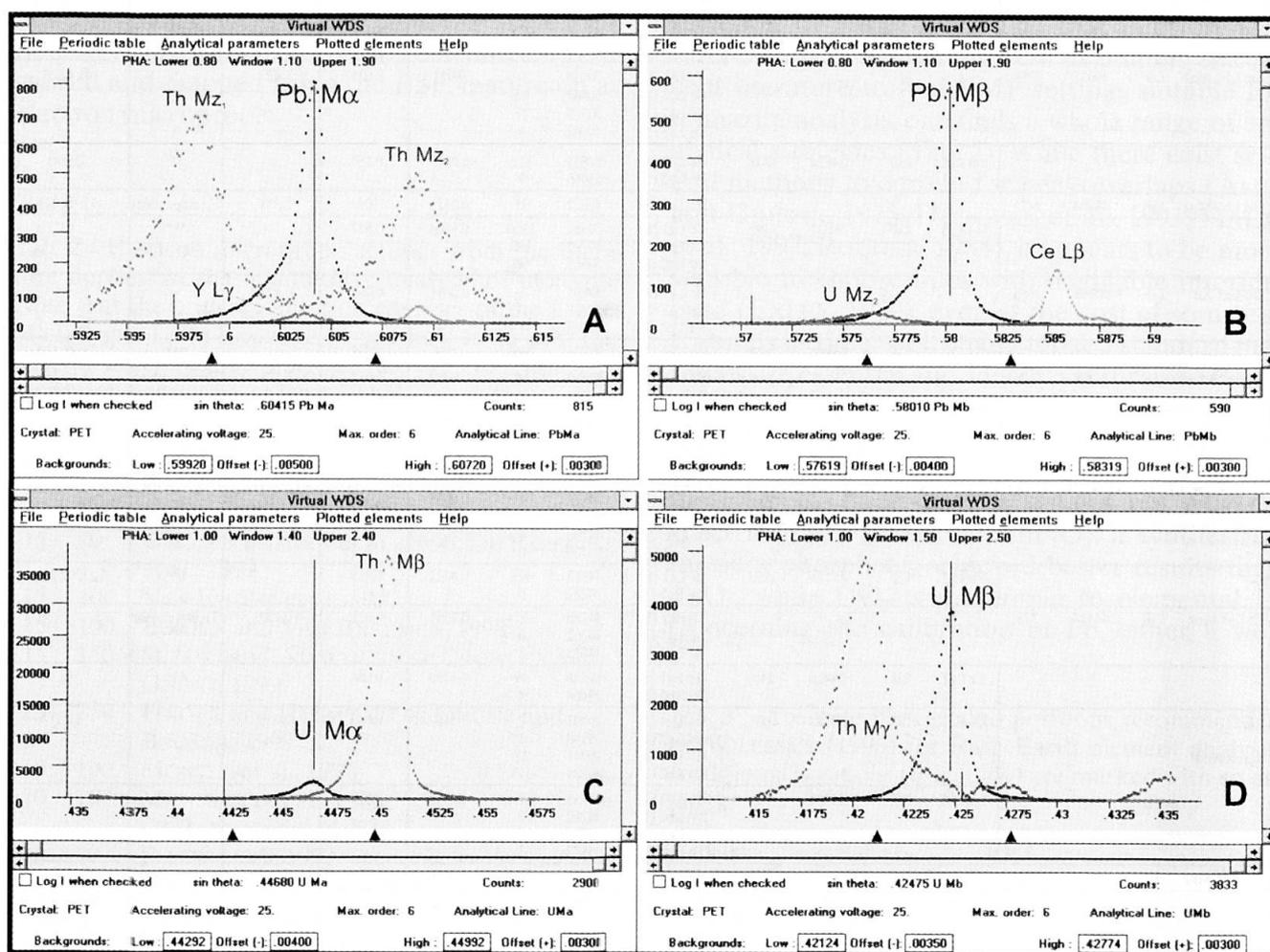

Fig. 4 Peak overlap simulations applying the program VIRTUAL WDS by REED and BUCKLEY (1996). These simulations were run with the monazite composition given in table 5. The figure visualizes the critical interferences relevant to Th-U-Pb dating of monazite with the EMP. Peak counts of the element of interest and interfering counts are listed in table 4.

Tab. 5 Reference composition of monazite and xenotime used for the calculations on table 4 and 6.

Monazite:			Xenotime:		
Elem.	Ions	wt%	Elem.	Ions	wt%
P	3.774	12.373	P	4.024	15.521
Si	0.278	0.825	Si	0.007	0.025
Ca	0.289	1.225	Ca	0.003	0.016
Y	0.222	2.076	Y	3.207	35.324
La	0.667	9.757	La	0.001	0.01
Ce	1.379	20.352	Ce	0.002	0.031
Pr	0.145	2.155	Pr	–	–
Nd	0.448	6.806	Nd	0.004	0.075
Sm	0.122	1.927	Sm	0.004	0.078
Gd	0.082	1.351	Gd	0.076	1.471
Tb	0.011	0.178	Tb	0.04	0.79
Dy	0.041	0.709	Dy	0.336	6.76
Ho	0.002	0.038	Ho	0.064	1.317
Er	0.007	0.132	Er	0.155	3.215
Yb	0.002	0.028	Yb	0.076	1.627
Lu	0.001	0.016	Lu	–	–
Pb	0.012	0.269	Pb	–	–
Th	0.499	12.251	Th	–	–
U	0.022	0.555	U	0.002	0.06
O	16	27.098	O	16	32.019
Sum	8.003	100.121	Sum	8.001	98.339

Tab. 6 This table demonstrates the effect of the overlaps on Pb Ma (Th Mz) and U Mb (Th Mg) with respect to Th-U-Pb age calculation. The monazite composition is listed in table 5. The ages have been calculated according to MONTEL et al. (1996).

PbO	ThO2	UO2	Analytical X-ray	line	Age Ma
0.290	13.941	0.630	Th Ma, Pb Mb, U Mb	corr	426
0.290	13.941	0.677	Th Ma, Pb Mb, U Mb	uncorr	422
0.290	13.941	0.818	Th Ma, Pb Mb, U Ma	uncorr	411
0.322	*13.941*	*0.630*	*Th Ma, Pb Ma, U Mb*	*corr*	*473*
0.322	*13.941*	*0.677*	*Th Ma, Pb Ma, U Mb*	*uncorr*	*468*
0.322	*13.941*	*0.818*	*Th Ma, Pb Ma, U Ma*	*uncorr*	*456*

select the most favorable lines. Table 6 demonstrates the effect arising from the neglect of interferences, using the monazite composition listed in table 5. Even though overlaps on Pb Ma and U Ma are counteracting, the calculated age is still 30 Ma off the best approximation (426 Ma) by using Pb Mb and correcting for interferences on U Mb.

Recommended settings for the quantification of monazite by electron microprobe are listed in table 8. These contain the full information on best lines, background positions, and integration times – optimized for a monazite composition as given in table 5. For compositions deviating considerably from the given example, adjustments may become necessary, as, for example, a simulation on VIRTUAL WDS would elucidate. Note that the

Tab. 7 Simulation of the Th Mg overlap on U Mb using the program VIRTUAL WDS for varying Th amounts in monazite for the determination of a correction factor based on Th Ma. The correction should be applied as follows:

U wt%$_{corrected}$ = U wt%$_{measured}$ – (0.0052 * Th wt%$_{measured}$).

Th wt%	I Th Mg at U Mb cps	I Th Ma pk cps	I Th shoulder / I Th Ma pk
5	117	22411	0.005221
10	235	44821	0.005243
11	258	49304	0.005233
25	587	112054	0.005239
30	704	134464	0.005236
Correction factor			0.00523

integration times and background positions are different for calibration on standards and measurement on monazite. All lines and background positions have been checked for interferences by means of wavelength dispersive scans and by applying the program VIRTUAL WDS, using the compositions of the natural monazite listed on table 5 and respective standard materials. Employing the settings outlined, correction procedures as introduced by ÅMLI and GRIFFIN (1975) are only applicable to the interference of Th Mg on U Mb (Tab. 7). All other elements listed using the respective lines and background positions have minimal overlaps or none for monazite similar to the reference sample. The elements Fe and Al are measured to have a control on the influence of adjacent minerals, and for good monazite analyses should fall below the detection limit of the EMP. With the recommended settings, 95% of 1000 analyses achieved totals of 98.00 to 101.00%, and 75% had cation sums within 7.99 and 8.02, normalizing to 16 oxygens.

BSE imaging and X-ray mapping

Monazite may show complex zonation patterns with domains of distinctive origin (COCHERIE et al., 1998; HAWKINS and BOWRING, 1997). Heterogeneity in the Th/Pb ratio is crucial to Th-U-Pb age interpretation and may reveal multi-stage growth, possible Pb diffusion, or partial recrystallization of a monazite grain. Thus, if monazite is to provide geochronological information, they ought to be tested for their growth topology. This is easily accomplished through BSE imaging of each grain prior or after quantitative analysis. The video settings for best imaging quality of zonation patterns vary from microprobe to microprobe and from grain to grain within one thin section. Recommended electron beam settings for BSE_Z

Tab. 8   Recommended settings for the quantitative analysis of monazite by EMP. Note that background positions and integration times are different for standardization and measurement. Ideally, standard materials for elements Y to Yb should be REE-phosphates (e.g. JAROSEWICH and BOATNER, 1991). U Mb and Th Mg are overlapping and adjustments should be made according to table 7.

Electron Microprobe: MPI Bern, Cameca SX 50 Accelerating Voltage: 25 kV; Beam Current: 50 nA											
Monazite analysis:				Measurement settings				Calibration settings			
Element	Val.	Line	X-tal	+ Bkg	– Bkg	Pk time	Bkg total	+ Bkg	– Bkg	Pk time	Bkg total	#Standard
P	5+	Ka	PET	1150	–1150	30	30	1150	–1150	30	30	CePO4
Al	3+	Ka	TAP	500	–500	30	30	500	–500	30	30	anorthite
Si	4+	Ka	TAP	500	–500	30	30	500	–500	30	30	almandine
Ca	2+	Ka	PET	500	–500	30	30	500	–500	30	30	anorthite
Y	3+	La	PET	500	–500	60	60	500	–500	60	60	Y2O3
La	3+	La	LiF2	700	–500	100	100	700	–500	100	100	La0.95Nd0.05 TiO3
Ce	3+	La	LiF2	650	–550	100	100	650	–550	100	100	CePO4
Pr	3+	Lb	LiF	8659	–441	50	50	500	–500	80	80	PrAlO3
Nd	3+	Lb	LiF2	1841	–2104	100	100	300	–350	80	80	†REE2
Sm	3+	Lb	LiF	2082	–4223	50	50	500	–500	80	80	†REE2
Gd*	3+	Lb	LiF	5841	–464	50	50	350	–300	80	80	†REE1
Tb*	3+	Lb	LiF	1272	–5628	50	50	400	–300	80	80	†REE1
Dy	3+	Lb	LiF	2919	–1145	50	50	450	–300	80	80	†REE4
Ho	3+	Lb	LiF	4483	–2417	50	50	500	–300	80	80	†REE4
Er	3+	La	LiF	1086	–2980	50	50	500	–500	80	80	†REE4
Yb	3+	La	LiF	none	–200	50	50	450	–300	80	80	†REE2
Lu	no ideal line											
Pb	2+	Mb	PET	4490	–7130	300	300	500	–500	50	50	crocoite
Th	4+	Ma	PET	400	–500	100	100	400	–500	50	50	ThP2O7
U	4+	Mb	PET	3390	–1505	150	150	500	–500	50	50	UO2
Fe	2+	Ka	LiF2	500	–500	30	30	500	–500	50	50	almandine
A* Xenotime analysis:												
Gd	3+	La	LiF	869	–5431	50	50	500	–500	50	50	†REE1
Tb	3+	La	LiF	2615	–3685	50	50	450	–300	80	80	†REE1
† standards by DRAKE and WEILL (1972) # Note that ideal standards for the elements Y to Yb are REE PO4, eg. by JAROSEWICH and BOATNER (1991).												

Conclusions

imaging are 15 kV and 20 nA, whereas for X-ray mapping of heavy elements, higher voltages and currents are preferable (e.g. 25 kV and 100 nA). While X-ray mapping can provide element specific maps within hours rather than seconds, BSE_Z images show the variation of the mean atomic number across the grain within a few seconds. Experience shows that patterns visible in BSE_Z images closely match X-ray maps of the element Th. Very little contrast is visible in X-ray maps of the elements Ce, La, Nd, Sm or Gd, mainly because the variation in Th is being compensated by several LREE (light rare earth elements). Monazite grains with no visible zonation in BSE_Z mode may thus be assumed as being homogeneous in chemistry and age within geologic times. Heterogeneity may potentially hint at multi-stage growth, even though this must not always be the case, an example being shown in figure 5.

Several conclusions regarding technical aspects of monazite analysis can be drawn from this research:

Lead-free thin sections required for Th-U-Pb analysis can be prepared using specially treated polyethylene disks for polishing – at no compromise in quality or efficiency.

Monazite is most easily analyzed by means of an electron microprobe which offers the combination of efficient searching, zonation imaging, quantification, and Th-U-Pb chemical dating capabilities. Neither optical microscopy, optical spectroscopy, alpha sputtering, cathode luminescence, UV luminescence or scanning electron microscope techniques can match the efficiency and the combination of tasks available on an electron microprobe.

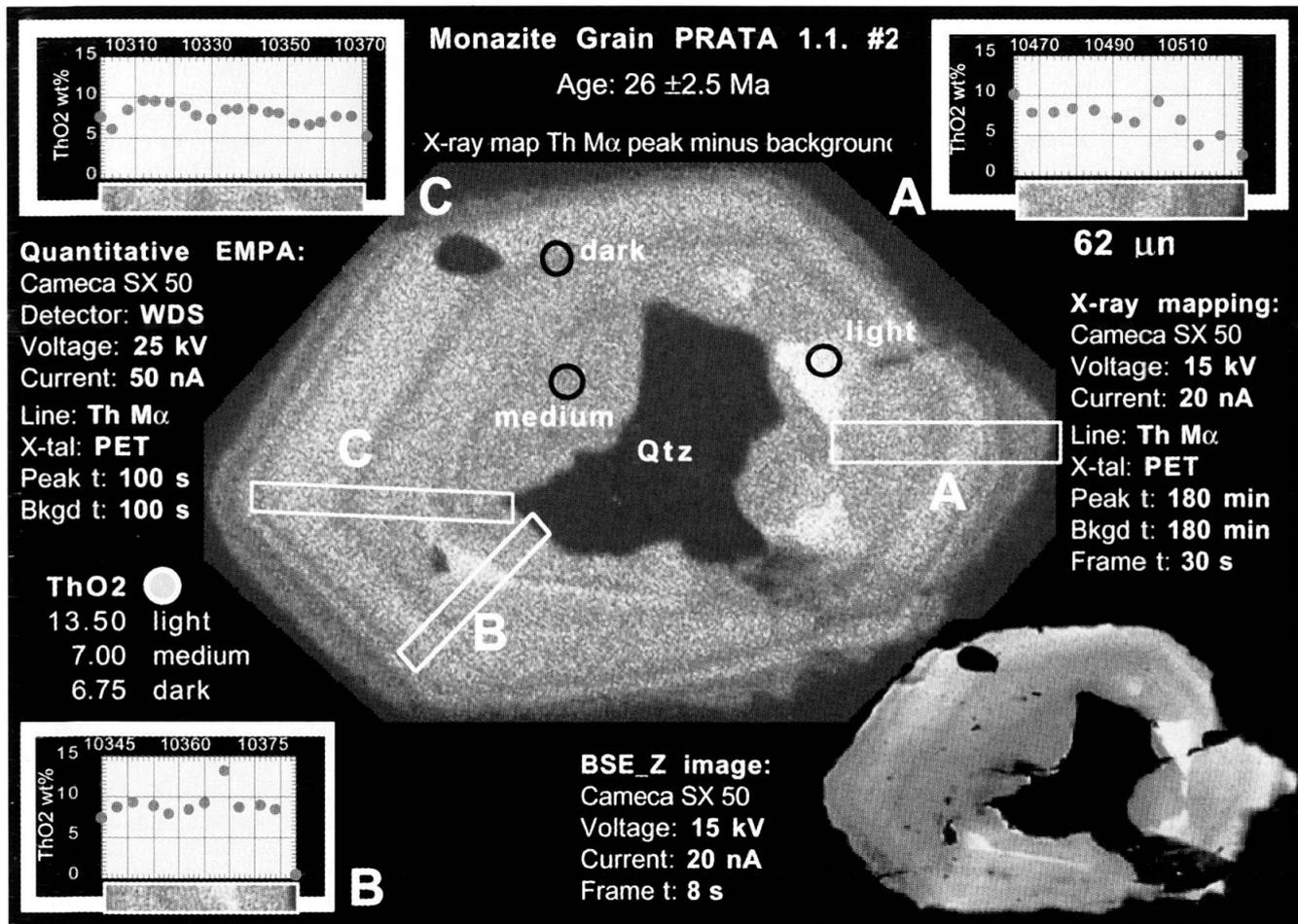Age information on monazite should only be interpreted upon tests on homogeneity using BSE_Z imaging facilities.

Fig. 5 Comparison of visualization methods to demonstrate variable Th contents within a zoned monazite grain. The grain (supplied by V. Köppel) has been dated by XRF-microprobe to 26 ± 2.5 Ma.

Quantification of monazite using wavelength dispersive spectrometry is time consuming and requires careful selection of analytical settings. Several misconceptions from the literature have been outlined and discussed, and for the first time a complete analytical strategy has been presented. Of particular interest to Th-U-Pb dating should be the common neglect of interferences on Pb Mα and U Mb.

References

ÅMLI, R. and GRIFFIN, W.L. (1975): Microprobe analysis of REE minerals using empirical correction factors. Amer. Mineral., 60, 599–606.

ANDREHS, G. and HEINRICH, W. (1998): Experimental determination of REE distributions between monazite and xenotime: potential for temperature-calibrated geochronology. Chem. Geol., 149, 83–96.

BEA, F. and MONTERO, P. (1999): Behavior of accessory phases and redistribution of Zr, REE, Y, Th, and U during metamorphism and partial melting of metapelites in the lower crust: An example from the Kinzigite Formation of Ivrea-Verbano, NW Italy. Geochim. Cosmochim. Acta, 63, 1133–1153.

BERNSTEIN, L.R. (1982): Monazite from North Carolina having the alexandrite effect. Amer. Mineral., 67, 356–359.

BINGEN, B. and VAN BREEMEN, O. (1998): U-Pb monazite ages in amphibolite- to granulite-facies orthogneiss reflect hydrous mineral breakdown reactions: Sveconorwegian Province of SW Norway. Contr. Mineral. Petrol., 132, 336–353.

BRAUN, I., MONTEL, J.M. and NICOLLET, C. (1998): Electron microprobe dating of monazites from high-grade gneisses and pegmatites of the Kerala Khondalite Belt, southern India. Chem. Geol., 146, 65–85.

COCHERIE, A., LEGENDRE, O., PEUCAT, J.J. and KOUAMELAN, A.N. (1998): Geochronology of polygenetic monazites constrained by in situ electron microprobe Th-U total lead determination: Implications for lead behaviour in monazite. Geochim. Cosmochim. Acta, 62, 2475–2497.

CROWLEY, J.L. and GHENT, E.D. (1999): An electron microprobe study of the U-Th-Pb systematics of metamorphosed monazite: the role of Ph diffusion versus overgrowth and recrystallization. Chem. Geol., 157, 285–302.

DELLA VENTURA, G., MOTTANA, A., PARODI, G.C., RAUDSEPP, M., BELLATRECCIA, F., CAPRILLI, E., ROSSI, P. and FIORI, S. (1996): Monazite-huttonite solid-solutions from the Vico Volcanic Complex, Latium, Italy . Mineral. Mag., 60, 751–758.

DEMARTIN, F., PILATI, T., DIELLA, V., DONZELLI, S. and GRAMACCIOLI, C.M. (1991): Alpine monazite; further data. Canad. Mineral., 29, 61–67.

DONOVAN, J.J., SNYDER, D.A. and RIVERS, M.L. (1993): An improved interference correction for trace element analysis. Microbeam Analysis, 2, 23–28.

DRAKE, M.J. and WEILL, D.F. (1972): New rare earth element standards for electron microprobe analysis. Chem. Geol., 10, 179–181.

EVANS, J. and ZALASIEWICZ, J. (1996): U-Pb, Pb-Pb and Sm-Nd dating of authigenic monazite: Implications for the diagenetic evolution of the Welsh Basin. Earth Planet. Sci. Let., 144, 421–433.

EXLEY, R.A. (1980): Microprobe studies on REE-rich accessory minerals; implications for Skye granite petrogenesis and REE mobility in hydrothermal systems. Earth Planet. Sci. Let., 48, 97–110.

FIALIN, M., OUTREQUIN, M. and STAUB, P.F. (1997): A new tool to treat peak overlaps in electron-probe microanalysis of rare-earth-element L-series X-rays. Eur. J. Mineral., 9, 965–968.

FINGER, F. and BROSKA, I. (1999): The Gemeric S-type granites in southeastern Slovakia: Late Palaeozoic or Alpine intrusions? Evidence from electron-microprobe dating of monazite. Schweiz. Mineral. Petrogr. Mitt., 79, 439–443.

FINGER, F., BROSKA, I., ROBERTS, M.P. and SCHERMAIER, A. (1998): Replacement of primary monazite by apatite-allanite-epidote coronas in an amphibolite facies granite gneiss from the eastern Alps. Amer. Mineral., 83, 248–258.

FINGER, F. and HELMY, H.M. (1998): Composition and total-Pb model ages of monazite from high-grade paragneisses in the Abu Swayel area, southern Eastern Desert, Egypt. Mineral. Petrol., 62, 269–289.

FRANZ, G., ANDREHS, G. and RHEDE, D. (1996) Crystal chemistry of monazite and xenotime from Saxothuringian-Moldanubian metapelites, NE Bavaria, Germany. In: AYORA, C. (ed.): Fluid inclusions., 8, 1097–1118. Schweizerbart'sche Verlagsbuchhandlung (Naegele u. Obermiller), Stuttgart.

GRATZ, R. and HEINRICH, W. (1997): Monazite-xenotime thermobarometry: Experimental calibration of the miscibility gap in the binary system CePO4-YPO4 . Amer. Mineral., 82, 772–780.

HAWKINS, D.P. and BOWRING, S.A. (1997): U-Pb systematics of monazite and xenotime: Case studies from the Paleoproterozoic of the Grand Canyon, Arizona. Contr. Mineral. Petrol., 127, 87–103.

JAROSEWICH, E. and BOATNER, L.A. (1991): Rare-earth element reference samples for electron microprobe analysis. Geostandards Newsletter, 15, 397–399.

KINGSBURY, J.A., MILLER, C.F., WOODEN, J.L. and HARRISON, T.M. (1993): Monazite paragenesis and U-Pb systematics in rocks of the eastern Mojave Desert, California, U.S.A.; implications for thermochronometry. In: WATSON, E.B., HARRISON, T.M., MILLER, C.F. and RYERSON, F.J. (eds): Geochemistry of accessory minerals; papers presented at the Third V. M. Goldschmidt conference., 110, 147–167. Elsevier, Amsterdam, Netherlands.

MANNUCCI, G., DIELLA, V., GRAMACCIOLI, C.M. and PILATI, T. (1986): A comparative study of monazite specimens from the Alpine region. In: PREWITT, C.T. (ed.): Abstracts with program 1986; the Fourteenth general meeting of the International Mineralogical Association., 166.

MONTEL, J.M., VESCHAMBRE, M. and NICOLLET, C. (1994): Dating Monazite with the Electron Microprobe. Com. Rend. Acad. Sci., Serie II, 318, 1489–1495.

MOUGEOT, R., RESPAUT, J.P., LEDRU, P. and MARIGNAC, C. (1997): U-Pb chronology on accessory minerals of the Velay anatectic dome (French Massif Central). Eur. J. Mineral., 9, 141–156.

PAQUETTE, J.L., MONTEL, J.M. and CHOPIN, C. (1999): U-Th-Pb dating of the Brossasco ultrahigh-pressure metagranite, Dora-Maira massif, western Alps. Eur. J. Mineral., 11, 69–77.

PARRISH, R.R. (1990): U-Pb dating of monazite and its application to geological problems. Canad. J. Earth Sci., 27, 1431–1450.

PODOR, R. and CUNEY, M. (1997): Experimental study of Th-bearing LaPO4(780 degrees C, 200 MPa): Implications for monazite and actinide orthophosphate stability. Amer. Mineral., 82, 765–771.

RAPP, R.P. and WATSON, E.B. (1986): Monazite solubility and dissolution kinetics; implications for the thorium and light rare earth chemistry of felsic magmas. Contr. Mineral. Petrol., 94, 304–316.

ROEDER, P.L. (1985): Electron-microprobe analysis of minerals for rare-earth elements; use of calculated peak-overlap corrections. Canad. Mineral., 23, 263–271.

SPEAR, F.S. and PARRISH, R.R. (1996): Petrology and cooling rates of the Valhalla complex, British Columbia, Canada. J Petrol., 37, 733–765.

STÄHLI Flathoning AG, Sägestrasse 10, CH-2542 Pieterlen/Biel, Switzerland. Facsimile: +41 (0)32 376 0509.

SUZUKI, K. and ADACHI, M. (1994): Middle Precambrian detrital monazite and zircon from the Hida Gneiss on Oki-Dogo Island, Japan; their origin and implications for the correlation of basement gneiss of Southwest Japan and Korea. Tectonophysics, 235, 277–292.

WILLIAMS, C.T. (1996) Analysis of rare earth minerals. In: JONES, A.P., WALL, F. and WILLIAMS, C.T. (eds): Rare Earth Minerals: Chemistry, origin and ore deposits, 327–348. Chapman and Hall, London.

WILLIAMS, M.L., JERCINOVIC, M.J. and TERRY, M.P. (1999): Age mapping and dating of monazite on the electron microprobe: Deconvoluting multistage tectonic histories. Geology, 27, 1023–1026.

Appendix

FINDING MONAZITE WITH THE CAMECA SX50 ELECTRON MICROPROBE

The following procedure, based on the setup of the SX50 microprobe laboratory at MPI Bern (SP1: (hP) LiF/PET; SP2: (lP) LiF/TAP; SP3: (hP) LiF/PET; SP4: (lP) TAP/PC1; SP5: EDS), has crystallized to be very efficient and effective:

Generate a focused beam with a voltage of 25 kV and a beam current of 50 nA.

Change the detectors to BSE Z mode.

SX>m1 vs1

SX>vs1 bse z

Adjust the magnification to mag 400. This sets the field of view on M1 in BSE mode equal to the field of view of the optical image.

SX>mag 400

Set the beam to scanning mode TV.

SX>mode tv

Ensure the orientation of the optical image is equivalent to the one of the BSE image. If not, rotate it such that the two images are identical.

SX>rota

Move the spectrometers to the following lines:

SX>mov sp1 ce la

SX>mov sp2 fe ka

SX>mov sp3 p ka

SX>mov sp4 y la

Adjust the contrast/brightness settings of M1:

SX>vs1 manu

Use the following settings:

Offset: 270

Dark level: 50

Contrast Difference: 1

Gain: 60

Turn the reflected light source back on.

SX>light samp 5

The transmitted light source should be off at all times while running in BSE mode. When the beam is in fixed spot size mode (SX>mode fix), the transmitted light source may be quickly turned on to check the context of the grain of interest. Turn it off before you switch back to scanning mode (SX>mode tv).

Now systematically scan the thin section using the x-y-z-stage control. Thanks to the high sensitivity of the BSE detector and screen, the stage can be moved at full speed without missing out on any potential candidates. Scanning of a round 1" thin section takes about 15 minutes, including the programming of the positions of the monazite and xenotime grains of interest.

SX>move stage [a-z] save

The above settings filter out any other phases (black) and show monazite as bright spots or areas, with the complete outline of the grain luminescing. Xenotime (YPO4) is just detectable on the screen with the above settings, is however not quite as bright as monazite. Pyrite (FeS2) shows equivalent brightness to monazite but is immediately identified in reflected light (slightly golden reflectance). Zircon (ZrSiO4) may luminesce similarly to monazite in some samples (you may lower the offset to 260), however, it can be easily distinguished from monazite: (1) from its typical morphology showing elongate idiomorphic shapes; (2) luminescence on the screen may show only part of the grain; (3) in reflected light, zircon is brighter than monazite (monazite is similar to garnet in reflected light); (4) by quickly changing the beam to fixed spot size.

SX>mode fix

If the beam spot is luminescing on the grain, it is either a xenotime or a zircon. High counts on P and Y indicate a xenotime, low counts on any of the spectrometers set as above indicate a zircon. Note that the fixed beam spot is slightly offset to the top right of the cross.